Cerebral Cortex, October 2020;30: 5502–5516

doi: 10.1093/cercor/bhaa132
Advance Access Publication Date: 4 June 2020
Original Article

ORIGINAL ARTICLE

Differential Generation of Saccade, Fixation, and Image-Onset Event-Related Potentials in the Human Mesial Temporal Lobe

Chaim N. Katz[1,2,†], Kramay Patel[1,2,3], Omid Talakoub[1,4], David Groppe[1], Kari Hoffman[4] and Taufik A. Valiante[1,2,5,6,7]

[1] Krembil Research Institute, Toronto Western Hospital, Toronto, ON M5T 1M8, Canada, [2]Institute of Biomaterials and Biomedical Engineering, University of Toronto, Toronto, ON M5S 3G9, Canada, [3]Faculty of Medicine, University of Toronto, Toronto, ON M5S 1A8, Canada, [4]Department of Psychology, Vanderbilt University, Nashville, TN 37240, USA, [5]Division of Neurosurgery, Department of Surgery, University of Toronto, Toronto, ON M5S 1A1, Canada, [6]Institute of Medical Sciences, University of Toronto, Toronto, ON M5S 1A8, Canada and [7]Electrical and Computer Engineering, University of Toronto, Toronto, ON M5S 3G4, Canada

Address correspondence to Taufik A. Valiante. Email: taufik.valiante@uhn.ca.

[†]Chaim N. Katz and Kramay Patel contributed equally to this work

Abstract

Event-related potentials (ERPs) are a commonly used electrophysiological signature for studying mesial temporal lobe (MTL) function during visual memory tasks. The ERPs associated with the onset of visual stimuli (image-onset) and eye movements (saccades and fixations) provide insights into the mechanisms of their generation. We hypothesized that since eye movements and image-onset provide MTL structures with salient visual information, perhaps they both engage similar neural mechanisms. To explore this question, we used intracranial electroencephalographic data from the MTLs of 11 patients with medically refractory epilepsy who participated in a visual search task. We characterized the electrophysiological responses of MTL structures to saccades, fixations, and image-onset. We demonstrated that the image-onset response is an evoked/additive response with a low-frequency power increase. In contrast, ERPs following eye movements appeared to arise from phase resetting of higher frequencies than the image-onset ERP. Intriguingly, this reset was associated with saccade onset and not termination (fixation), suggesting it is likely the MTL response to a corollary discharge, rather than a response to visual stimulation. We discuss the distinct mechanistic underpinnings of these responses which shed light on the underlying neural circuitry involved in visual memory processing.

Key words: corollary discharge, event-related potentials, hippocampus, human intracranial electroencephalography, saccades

Introduction

The electrophysiological responses of mesial temporal lobe (MTL) structures, known for their critical role in memory, have been characterized using a variety of behavioral paradigms and described according to their temporal relationship to stimulus onset (i.e., image-onset, word presentation, etc.). Neural responses following image presentation have been reliably used to study memory processes (Fernandez et al.

1999; Tesche and Karhu 2000; Paller and McCarthy 2002; Fell et al. 2004, 2008; Sederberg et al. 2006; Montefusco-Siegmund et al. 2017), whereas, despite a rich literature linking eye movements to memory (for review, see Meister and Buffalo 2016), very few have investigated electrophysiological responses of human MTL structures to eye movements (Hoffman et al. 2013; Andrillon et al. 2015). At first glance, image-onset and saccadic eye movements both present salient information to visual centers, suggesting that subsequent processing would be similar, as would be the electrophysiological responses to them. Conversely, if such responses differ, it would suggest that their neural correlates differ and that tasks/analyses that preferentially favor analyzing responses to one or the other are capturing distinct visual and likely mnemonic processes.

Arguments can be made to support or refute why MTL electrophysiological responses to image-onset and saccadic eye movements might appear similar. Intuitively, since the hippocampus is a multimodal integrator far removed from the primary visual cortex, it may be agnostic as to how visual information arrives (Rey et al. 2015). In this context any new retinal information, independent of its generation, would result in the same electrophysiological response. The literature however suggests visual and oculomotor responses are likely to be different. For example, MTL responses to the presentation of images, which are consistently used for investigations in word paradigms (Fernandez et al. 1999; Fell et al. 2008), Sternberg probes (Tesche and Karhu 2000), and complex visuals (Paller and McCarthy 2002), are usually long latency responses with large amplitudes. (Paller and McCarthy 2002; Mormann et al. 2005; Andrillon et al. 2015). These MTL responses can be looked at through recognition, working memory or even recall tasks (presentation of first stimulus), with focus on the response to presentation of the visual stimulus. On the other hand, eye movement-related responses in the MTL tend to have a shorter latency and lower amplitude (Andrillon et al. 2015). In line with these findings are those of Bartlett et al. who specifically compared the responses within the macaque superior temporal sulcus, a region analogous to the human brain region responsible for integrating auditory and visual information (Beauchamp et al. 2004) to image presentation and eye movements (Bartlett et al. 2011). Their results suggested a clear distinction between image-onset and eye movement-related responses in the time and frequency domain, and that the image-onset response can be modulated by succeeding eye movements. The precise origin of eye movement-related ERPs is likely dependent on where recordings have been performed; nevertheless, there is indeed support for the concept that they in part represent a corollary discharge (CD). CDs represent a transformed copy of a motor command signal that informs sensory systems of impending motor activity, thereby distinguishing self-generated changes in sensory signals from the changes generated from the external world (Crapse and Sommer 2008). Such a signal can propagate widely throughout the brain, as well as through the ventral visual pathway and temporal lobe structures (Sommer and Wurtz 2002; Purpura et al. 2003). If indeed the MTL response to eye movements results in part from a CD, it would imply a fundamental mechanistic difference in how visual information is processed in mnemonic structures like the human hippocampus. However, it remains an open question whether the human mesial temporal lobe structures respond differently during these two processing conditions (i.e., image presentation and eye movements)—conditions that have substantial effects on memory and the corresponding electrophysiological measurements in the MTL (Paller and McCarthy 2002; Fell et al. 2008; Axmacher et al. 2010; Hoffman et al. 2013; Andrillon et al. 2015; Kleen et al. 2016).

A variety of invasive and noninvasive electrophysiological recording techniques have been used to study MTL physiology (Brewer et al. 1998; Jackson and Schacter 2004; Sederberg et al. 2006; Long et al. 2014; McCormick et al. 2015; Merkow et al. 2015). Intracranial electroencephalography (iEEG), unlike other recording modalities, provides access to neural activity with high spatial and temporal resolution allowing investigation of electrophysiological activity in deep structures at "fast" time scales (Johnson and Knight 2015). Such activity can be seen in single-trial events or averaged across trials aligned to events/stimuli to obtain event-related potentials (ERPs) (Davis 1939). ERPs can be then further decomposed into their respective frequency components, to associate increases/decreases in power/phase clustering to various memory processes (Paller and McCarthy 2002; Fell et al. 2008; Axmacher et al. 2010; Kleen et al. 2016), and have been used to infer putative neuronal mechanisms like phase resetting (Fell et al. 2004; Klimesch et al. 2006; Hanslmayr et al. 2007; Canavier 2015). The study of ERPs has thus contributed significantly to our understanding of MTL function by allowing the attribution of changes in timing, amplitude, and spatial organization of brain-related activity to putative cellular mechanisms thought to underlie the generation of such specific electrophysiological signatures (Womelsdorf et al. 2014).

ERPs are widely thought to be generated by either (1) stimulus-specific firing of additional neurons (evoked responses) or (2) poststimulus phase alignment of ongoing neural oscillations without additional neuronal firing (phase-reset response) (Makeig et al. 2002; Shah et al. 2004; Sauseng et al. 2007). Broadly speaking, the primary and most basic distinction between these two mechanisms is that evoked responses demonstrate an increase in individual trial power poststimulus onset, whereas phase-reset responses do not (Shah et al. 2004). Identifying which of these putative mechanisms underlies a specific ERP not only characterizes the neuronal response but also suggests what physiological processes underlie the response. For instance, in the auditory cortex of animals, ERPs arising from somatosensory stimulation appear as a phase reset, arising from the "modulation" (Sherman and Guillery 2002) of the timing of neuronal activity within the auditory cortex, without an increase in excitability (Schroeder and Lakatos 2010). This preferential alteration of the timing of neuronal activity through phase resetting is thought to be important in plasticity mechanisms and transmission of information within the nervous system (Axmacher et al. 2006; Canavier 2015; Voloh and Womelsdorf 2016). Conversely, ERPs within the auditory cortex from auditory stimulation appear as an evoked response, resulting from "driving" (Sherman and Guillery 2002) increases in neuronal excitability (Schroeder and Lakatos 2010). Therefore, the characterization of ERPs following image presentation and eye movements using this framework can provide mechanistic insights to MTL electrophysiological responses.

Thus, to begin understanding the neural correlates of image-onset and eye movement-associated ERPs in humans, MTL responses to image-onset and eye movements were characterized and compared in epilepsy patients undergoing iEEG investigations using a scene recognition task previously shown to have medial temporal lobe dependency (Chau et al. 2011). Intertrial phase clustering (ITPC) and spectral power were used to compare MTL electrophysiological responses to

Table 1 Patient summary table. Data for each participant are shown in the respective rows. Rows highlighted in black identify patients who were not analyzed due to insufficient data and poor eye-tracker calibration

ID	Sex	Age	Resection	PH	HIPP	# Saccades	Median saccade duration (ms)	Median fixation duration (ms)	# Blocks completed
P14	F	28	RAT	2	0	12 281	16	225	9
P15	M	44	RAT	1	2	1909	75	109	2
P16	F	39	RAT	2	4	16 676	17	151	11
P17	F	32	NA	1	2	3177	9	242	2
P18	M	28	NA	1	1	17 894	9	267	12
P19	M	32	NA	4	1	4739	9	501	9
P20	M	36	NA	1	2	14 508	9	300	12
P21	F	25	RAT	2	0	20 717	16	217	12
P22	M	31	NA	1	2	808	192	108	3
P25	F	45	RAT	1	2	16 701	9	276	12
P26	F	58	NA	2	3	11 267	9	259	6

saccadic eye movements and image-onset. We demonstrate that the MTL responses following image-onset and saccade-onset events are starkly different with the former being a primarily evoked response showing within-trial power increases and phase clustering in lower frequency bands (delta and low theta) and the latter being best described as a phase reset in the delta/theta/alpha frequency bands with significant phase clustering in the absence of within-trial power increases. We further demonstrate that saccade-associated ERPs are initiated with saccade onset and not fixation, suggesting that the ERP associated with saccadic eye movements is initiated before retinal reafference, suggesting it is an internally generated signal like a CD (Purpura et al. 2003; Andrillon et al. 2015).

Methods

Method Details

Subject Details

This study reports data from 11 subjects (6 females, 36.2 ± 9.7 years of age) with medically refractory epilepsy, who were implanted with subdural surface electrodes and depth macroelectrodes to localize epileptogenic regions (Table 1). Electrode locations were selected strictly on clinical grounds. These experiments were performed between 2 and 10 days postoperatively. All research was performed in accordance with protocols approved by the University Health Network Research Ethics Board.

Experimental Design

The experimental design of this study is identical to that described previously (Hoffman et al. 2013). A summary is provided here. Participants were seated comfortably in their hospital beds and performed the task on laptop computer. For each trial, an original scene (taken from a large collection of natural scenes including landscapes, wildlife, cityscapes, and indoor scenes) was shown at a full resolution of 1280 x 1024 and alternated with a target-modified scene every 500 ms, with a 50 ms gray screen separating these images. The target-modified scene was always a modified version of the original scene, in which one object in the scene (here called the "target") was modified in Adobe Photoshop to give the impression that it disappeared. The size, location, and content of these targets were modified between different scenes to reduce predictability. Participants were asked to search for the target in each pair of alternating images and could elicit the end of the trial by fixating their eyes on the target for a period of 1000 ms. Once they found the target, or after a time limit of 45 seconds, the trial ended with revealing the target by rapidly altering between the two images without the gray screen gap. Trials were presented in blocks of 30, and each participant participated in up to 12 such blocks of data collection. Each scene pair was either novel or repeated once from a previous trial, with equal probability. Between trials in each block, participants were presented with a series of screens asking for verbal responses for the memory of the scenes and targets. Behavioral data from the intertrial period are not presented or discussed here. An overview of the task and stimuli presentations is presented in Figure 1A,B.

Eye-Tracking Analysis

Eye tracking was performed using the iView RED eye-tracking system. The eye tracker was placed at the bottom of the screen, while patients were seated comfortably in their hospital beds, with the screen placed approximately 60 cm from their eyes. All participants first underwent a nine-point calibration of the eye-tracker system. The eye tracker was connected via a USB cable to the laptop computer on which the behavioral task was presented. It was interfaced using the same software (NBS Presentation) that was used to present the task. Eye-tracking data were preprocessed to identify saccade and fixation events using the iView X iTools IDF Event Detector (SensoMotoric Instruments, Teltwo, Brandenburg, Germany). Fixation events were detected by this commercial software using an identification by dispersion threshold (IDT) algorithm. This algorithm uses two fixed thresholds: a maximum fixation dispersion threshold (100 pixels) and the minimum fixation duration threshold (80 ms) (Salvucci and Goldberg 2000). To be considered a fixation, the gaze must stay within the dispersion threshold for at least the specified duration threshold. The end of each fixation event is marked as a saccade event. This saccade and fixation events detected with this algorithm have been shown to be robust for low-sampling eye trackers. In a comparative analysis of 10 eye-tracking algorithms, the IDT algorithm used here was shown to be second closest to human detection for saccade events (Andersson et al. 2017). A sample of fixations detected is presented in Figure 1C.

Neural Recordings

Electrophysiological data presented here were recorded using depth macroelectrodes with four electrical contacts placed to

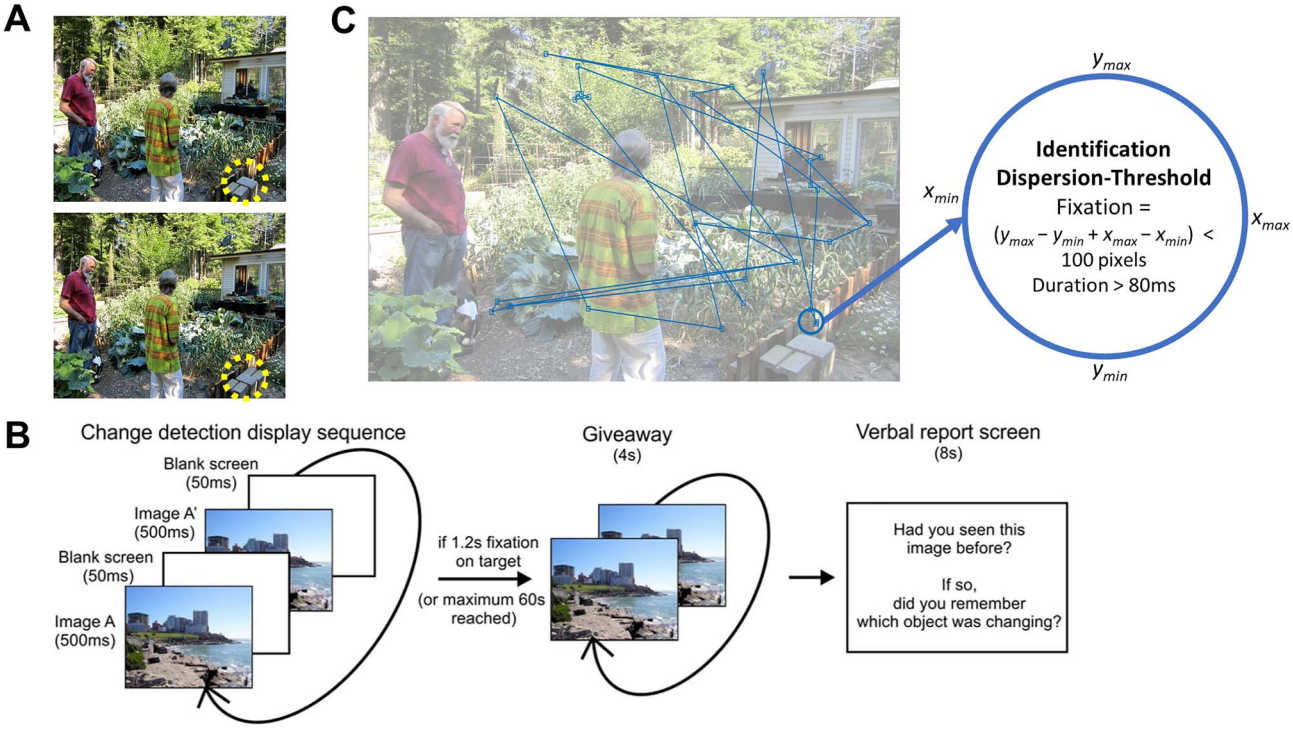

Figure 1. Behavioral task and fixation detection. (*A*) Sample visual stimulus with target objects such as a disappearing plant shown circled in yellow. (*B*) A trial sequence which shows the image switching between the two stimuli for target search. Giveaway is when the target is found, or time has passed, and participants then report on whether or not they have seen image. (*C*) Fixation events from a sample subject. Each fixation event is detected using an algorithm provided by the manufacturer of the eye tracker. As can be seen here, a fixation must stay within the 100 pixel dispersion for at least 80 ms to be considered a fixation event. The end of a fixation event is considered the start of the subsequent saccade.

record hippocampal activity. A four-contact subgaleal electrode was used for ground and reference and was placed over the parietal midline facing away from the brain. Signals were sampled at 5 kHz, and hardware filtered from 0.1 to 1 kHz, with a NeuroScan SynAmps2 data acquisition system (Compumedics, Charlotte, NC, USA). Neural data were synchronized with eye-tracking data with the use of TTL triggers sent from the laptop computer to the NeuroScan computer. Electrode localization was performed by coregistering pre-op MRI with post-op CT using the iELVIS toolbox (Groppe et al. 2017). Following localization, the precise location of each of the four hippocampal electrodes was determined. Only those labeled as parahippocampal or proper hippocampal, and later verified by a neurosurgeon, were analyzed further. All electrophysiological data were preprocessed by bandpass filtering between 0.5 and 200 Hz using second-order Butterworth filter, downsampling to 1 kHz, and notch filtering at 30 and 60 Hz to remove line noise and artifacts. All further analysis was performed using custom-written scripts in MATLAB (The Mathworks Inc, Natick, MA, USA).

Data Analysis

Event-Related Potentials

To obtain ERPs for image-onset events, iEEG data from all trials and all relevant electrodes were aligned to the initial image-onset and trimmed to epochs containing 1.6 s of data before and after each event. The ERP for each electrode was then obtained by taking the mean of these image-onset epochs across all trials from all experimental blocks (1 image-onset event per trial X 30 trials per blocks X up to 12 blocks per subject = ~360 image-onset events for each ERP). Fixation and saccade ERPs were obtained in a similar manner (±1.6 s around saccade and/or fixation onset) from the period following image-onset, up until the end of the trial (when the target is found or revealed). As such, only saccades and fixations during the active visual search are used for analysis here. It should be noted that the temporal alignment of the ERPs is limited by the sampling frequency of the eye tracker (i.e., 120 Hz) and the refresh rate of the display (i.e., 60 Hz). This resolution may introduce some temporal jitter into the subsequent analysis, preventing elicitation of higher frequency phase clustering (if such were to exist).

Alignment of ERPs to Fixation or Saccade Events

The extremely rapid nature of saccades (median length of 9 ms across all subjects) makes it difficult to distinguish between a saccade-aligned ERP and a fixation-aligned ERP (Fig. 2A). To determine whether the observed saccade-aligned ERPs and fixation-aligned ERPs were distinct events, or the same event viewed from different time points, the saccade-aligned and fixation-aligned ERPs were calculated for varying saccade durations. To do this, saccade and fixation epochs were binned based on the duration of the saccade succeeding the saccade-onset and preceding the fixation onset. Considering the eye-tracker sampling rate of 120 Hz, the first bin was centered at 8 ms with a width of 8 ms. Succeeding bins were separated by 8 ms and had the same width. Saccade lengths >56 ms were not analyzed for the sake of this comparison because of the small number of saccades in each succeeding bin. Fixation and saccade-aligned

ERPs were then obtained by averaging all the epochs within each bin. These ERPs were then normalized by z-scoring (to control for the varying number of epochs in each bin) and plotted on a contour plot (Fig. 2C for saccade-aligned ERPs and Fig. 2D for fixation-aligned ERPs), with varying saccade durations on the y-axis and time relative to saccade-onset (Fig. 2C) or time relative to fixation onset (Fig. 2D) on the x-axis.

Saccadic Transient Analysis and Removal

The saccade ERPs across all subjects appeared to have a transient peak around saccade onset, hereafter referred to as the peri-saccadic transient. Recent studies suggest that iEEG recordings may be contaminated with an oculomotor artifact resulting from the contraction of extraocular muscles which facilitate eye movements (Jerbi et al. 2009; Kovach et al. 2011). To remove this artifact from further analysis, we employed a slightly modified procedure for removal of this eye movement artifact as described by Kovach et al. (2011). More specifically, we used independent component analysis on all the mesial temporal lobe electrodes implanted in each patient (between 8 and 12 electrodes per patient) using the Bell–Sejnowski ICA algorithm (Bell and Sejnowski 1995) implemented in the EEGLab toolbox for MATLAB (Delorme and Makeig 2004). The resulting components were used one at a time to reconstruct the original data, and the variance-accounted-for (VAF) measure between the reconstructed signal and the original signal was calculated for each of these reconstructions as shown in equation (1):

$$\mathrm{VAF} = \frac{\mathrm{var}\ (X_{\mathrm{original}} - X_{\mathrm{reconstructed}})}{\mathrm{var}\ (X_{\mathrm{original}})} \quad (1)$$

Here, X_{original} is the original signal with the peri-saccadic spike, and $X_{\mathrm{reconstructed}}$ is the signal reconstructed with each component, and var defines the variance of the signal. This VAF measure was only calculated for a 40 ms window around each saccade event, to isolate the importance of each component towards generating the peri-saccadic transient. The VAF measure was then averaged for all saccades, and across all MTL electrodes for each reconstruction, and then ranked from largest to smallest for all the components. Based on this ranking, the two components with the largest contribution to the peri-saccadic transient were tagged for removal. Removing the entire component significantly affected the entire ERP waveform for the different electrodes. Thus, in an effort to preserve as much of the signal as possible, a moving average interpolation was performed on the two selected components, on a 40 ms window around each saccade (±20 ms) (Abel et al. 2016). The two modified components with the spikes removed were then used along with the nonmodified components to reconstruct the original data, but with the peri-saccadic transient removed. This reconstructed data are referred to as the ICA-filtered data in all further analysis.

Phase-Reset Simulations

To test the hypothesis that the peri-saccadic transient is part of the physiological hippocampal response to eye movements and not just an EOG artifact, simple simulations were performed to determine whether such a rapid transient response could be generated by physiological neural mechanisms. Prior work has suggested that the hippocampal response to eye movements

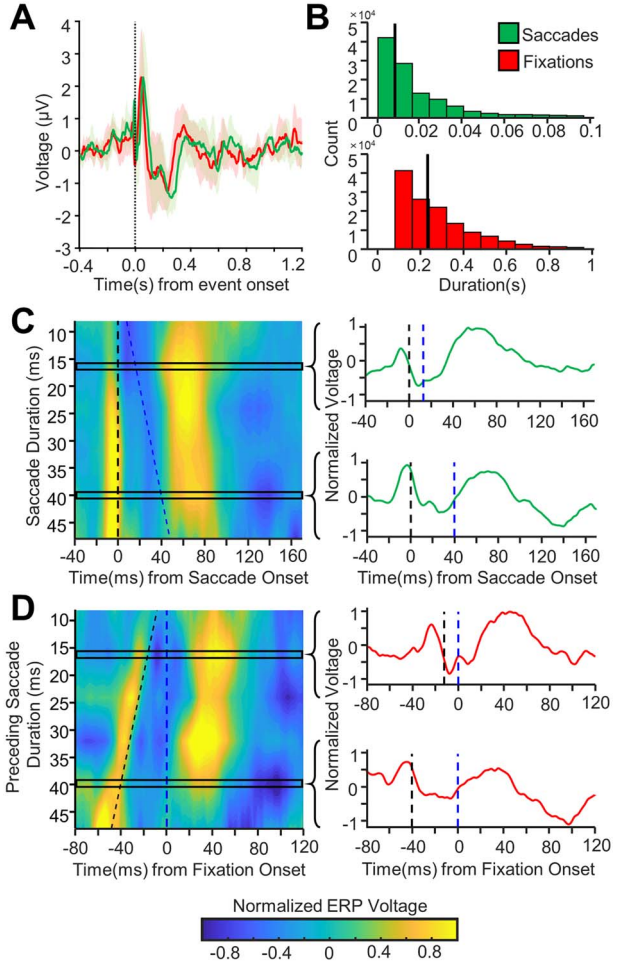

Figure 2. Saccade versus fixation alignment of hippocampal response to eye movements. (*A*) Grand-average hippocampal ERP aligned to fixation (red) or saccade (green) onset (mean ± 95% confidence intervals). (*B*) Histogram of fixation and saccade lengths across all patients and trials. The vertical black line marks the median fixation and saccade duration respectively. (*C*) Left: Contour plot showing grand-average saccade-aligned ERPs for changing saccade durations (shorter saccade durations towards the top of the graph, longer durations towards the bottom) for all hippocampal electrodes. The x-axis shows time relative to saccade onset. Saccade onset is marked by the dashed black vertical line. Fixation onset is marked by the dashed blue line. Note that as the saccade duration changes, the response remains aligned to the saccade onset. Each response to saccade duration ERP appears to have a rapid voltage response at saccade onset likely due to extraocular muscle contractions (along the black dotted line), further discussed in the results under Analysis and Removal of the Peri-saccadic Transient. Right: the normalized ERP waveforms for two different rows of the contour plot is shown with the saccade onset marked with a dashed black line and fixation onset marked with the dashed blue line. Note, the saccade ERP is very similar for saccades of different durations across all electrodes. (*D*) Left: As C but for fixation-aligned ERPs. The y-axis shows the duration of saccade preceding the fixation. The x-axis shows time relative to fixation onset. Fixation onset is marked with the dashed blue line, and saccade onset is marked with the dashed black line. Right: the normalized ERP waveforms for two different rows of the contour plot are shown with the saccade and fixation onsets marked as before. Note that as the saccade duration changes, the waveform shifts to remain aligned with saccade onset.

(saccades or fixations) is generated by a phase-reset or clustering mechanism, in which ongoing oscillators, in the theta frequency band, reset their phase following saccade or fixation onset. Hence, sinusoidal oscillators were simulated at every integer frequency from 1 to 200 Hz with a randomly assigned

phase. The amplitude of these oscillators was selected to match the power spectrum of the neural data recorded from a randomly selected hippocampal electrode. At time $t = 0$, the phase of the oscillators in the theta frequency band was instantaneously reset to a predetermined phase, whereas the other oscillators continued to oscillate in accordance with their earlier phase. Temporal and frequency jitters were added to each oscillator to simulate the dynamics of real neural oscillators and to ensure that the phase alignment of the oscillators would quickly dissipate following the phase reset. The simulated neural signal "recorded" form each trial was the sum of the outputs of each oscillator. A thousand such trials were generated for each phase reset, and an ERP was generated by summing the response across all of these trials.

Intertrial Phase Clustering

ITPC is a measure used to look at how the phase of oscillations clusters in the time-frequency domain. To calculate ITPC, the time-frequency representation of all saccade- and image-onset epochs was first obtained using a short-time fast Fourier transform (stFFT). Note that the saccade-onset epochs were derived from the ICA-filtered data. A Hanning window of 1000 ms, in steps of 10 ms, was used to reduce edge artifacts. Equation (2) was then used to obtain the ITPC value. Here, n is the number of epochs (saccade or image-onset) for each electrode, and θ_{rtf} is the phase angle of the rth epoch at time t and frequency f. The calculated value ITPC_{tf} is the ITPC value at a given time-frequency point:

$$\mathrm{ITPC}_{tf} = \left| \frac{1}{n} \sum_{r=1}^{n} e^{i\theta_{rtf}} \right| \quad (2)$$

Since there were a significantly larger number of saccade epochs for each electrode compared with image-onset epochs, comparing the ITPC values between these events would have been difficult given the impact the number of events has on the calculated ITPC value. To reduce the effect of the number of events on the ITPC values, the values were transformed to ITPC_z values, also known as Rayleigh's Z, as shown in equation (3):

$$\mathrm{ITPC}_z = n \times \mathrm{ITPC}^2 \quad (3)$$

Average ITPC_z values in five different, nonoverlapping time-frequency windows (delta [1–3 Hz), theta [4–8 Hz], alpha [9–14 Hz], beta (15–26 Hz), and low-gamma [27–80 Hz]) in the post- and pre-event periods were calculated for further statistical analysis. The time duration of each of these windows in the postevent period was selected such that at least one full oscillation of the mean frequency component of each window was captured (see Table 2 for the precise temporal definition of these windows). Pre-event windows were chosen to be the same time duration as the postevent windows and were chosen to end 0.2 s before the event onset, to avoid picking up any postevent activity present before the event onset due to temporal smearing that may occur due to the selected Hanning window.

Pre- and Post-Stimulus Power

spectral power was calculated for each individual epoch (saccade- and image-onset) using the previously obtained time-frequency representation and then averaged across all trials for each electrode (note that the saccade-onset epochs were derived from the ICA-filtered data). Similarly, spectral power was also calculated for each electrode-specific ERP. To investigate power changes in each trial and in each ERP, pre-event and postevent power was obtained for the five different frequency bands defined in Table 2, by averaging out the power in the pre-event and postevent windows. Log power change (reported in decibels) between the post- and pre-event windows was calculated using equation (4). Here, pre-event power refers to the average power in the pre-event time-frequency window, and postevent power refers to the average power in the postevent time-frequency window:

$$\text{Log power change (dB)} = 10 \times \log_{10}\left(\frac{\text{post} - \text{event power}}{\text{pre} - \text{event power}}\right) \quad (4)$$

Table 2 Time-frequency window definitions. This table shows the time-frequency windows that were used for analyzing the changes in ITPC and power following image-onset and saccade-onset in this paper. Note that for each frequency band, the pre- and post-event windows are of the same duration. However, the window lengths for different frequency bard are designed to include at least one cycle at the mean frequency of the frequency band of interest. Hence, the lower frequency bands (1–2 Hz) will have larger window sizes than the higher frequency bands. Also, note that the pre-event windows were chosen to end 200 ms before the onset of the event in an effort to avoid including any temporal smearing effects that may be present due to the short-time fast Fourier transform (stFFT) technique that was used to obtain the analytical signal

Frequency band	Pre-event window	Postevent window
Delta (1–3 Hz)	−800 to −200 ms	0–600 ms
Theta (4–8 Hz)	−600 to −200 ms	0–400 ms
Alpha (9–14 Hz)	−500 to −200 ms	0–300 ms
Beta (15–26 Hz)	−500 to −200 ms	0–300 ms
Gamma (27–80 Hz)	−400 to −200 ms	0–200 ms

Quantification and Statistical Analysis

Rejected Data

Experimental data were originally collected from 11 subjects, which contributed data from 19 hippocampi and 18 parahippocampi (Table 1). Note that data collected from hippocampi/-parahippocampi that were later found to be in the seizure onset zone were not analyzed in this study and are not included in the counts provided in Table 1. Data from two of the subjects had to be rejected however due to poor eye-tracker calibration, incomplete experimental blocks, and insufficient data. Hence, the data reported here are from 15 hippocampal electrodes from seven different subjects and 16 parahippocampal electrodes from nine different subjects. Note that for all population-level statistical analysis performed in this study, data points were marked as outliers using the Tukey method (Tukey 1977) which is described as follows:

$$\text{Low outliers} = Q_1 - 1.5\,(Q_3 - Q_1) = Q_1 - 1.5\ (\mathrm{IQR}) \quad (5)$$

$$\text{High outliers} = Q_3 + 1.5\,(Q_3 - Q_1) = Q_3 + 1.5\ (\mathrm{IQR}) \quad (6)$$

Event-Related Potentials

To determine the significance of each ERP, a representative distribution of ERP maxima and minima was obtained for each electrode/ERP using nonparametric permutation testing with randomized polarity inversions (3000 permutations). ERP values

were deemed significant if they fell above the 97.5th percentile of the distribution of maxima or below the 2.5th percentile of the distribution of minima.

Intertrial Phase Clustering

Within-Electrode Analysis

Initial, within-electrode significance of each $ITPC_z$ value was obtained using equation (6), where n was the number of epochs used to obtain the ITPC values. This initial significance was then corrected for multiple comparisons using the Benjamini–Hochberg FDR correction at the $\alpha < 0.001$ significance level. Significant portions were then masked for visualization (Fig. 4A):

$$p_{\text{initial}} = e^{-n\times \text{ITPC}^2} = e^{-\text{ITPC}_z}$$

Between-Electrode Analysis

Between-electrode statistical analysis was performed to quantify the change in phase clustering in the postevent period compared with the pre-event period. To do this, specific time-frequency windows in the pre- and post-onset period for each event were defined, as shown in Table 2, and described earlier. The average $ITPC_z$ values from these windows were compared between all electrodes using a paired, two-tailed T-test, corrected for multiple comparisons using the Benjamini–Hochberg FDR correction at the $\alpha < 0.01$ level.

Spectral Power Analysis

The average power in the pre- and post-event period was obtained for five different frequency bands described earlier and shown in Table 2. The log power change was then calculated for each frequency band using equation (4). A two-tailed, one-sample T-test was used to test the null hypothesis of zero power change following event onset. The significance values obtained using these tests were corrected for multiple comparisons using the Benjamini–Hochberg FDR correction at the $\alpha < 0.01$ significance level.

Results

Visual Search Behavior

We used a previously reported behavioral paradigm (a change-blindness task) with a new set of participants that incorporates image-onset and saccadic search and has been shown to be MTL dependent (Chau et al. 2011) with neuronal correlates to search and memory localized to the hippocampus (Leonard et al. 2015; Leonard and Hoffman 2017; Montefusco-Siegmund et al. 2017) (Fig. 1). In this task, scenes were presented with the goal of finding the changing object in the scene. At the start of each trial, each participant fixated on a fixation cross in the middle of the screen, after which a scene, with a hidden target, was presented, subsequently referred to here as image-onset (see Methods section for more details). All participants actively searched the scenes for the hidden target. Each participant contributed between 3000 and 21 000 saccades/fixations across all experimental trials (see Table 1). Saccades had a median duration of 9 ms, and fixations had a median duration of 242 ms (Fig. 2B). Local field potentials (LFPs) were recorded from 15 hippocampal electrodes from seven different subjects and 16 parahippocampal electrodes from nine different subjects (see Methods section; Table 1 for more details).

Fixation Versus Saccade Responses

Since previous literature makes little distinction between eye movement-related responses in the MTL aligned to saccade-onset or to fixation onset, these responses were analyzed here for both alignments. Saccade-aligned and fixation-aligned responses in the MTL were nearly identical (Fig. 2A). Saccade durations were very short (Fig. 2B), suggesting that the saccade-onset ERPs and the fixation-onset ERPs were the same ERP aligned to two different yet temporally proximal events. Although such short saccades are sometimes excluded from analysis or are considered to be microsaccades, they were included in the present analysis as they constituted a majority of the recorded saccades and to ensure that the results reported here were generalizable across all saccades (Corrigan et al. 2017). To determine whether the observed response was better aligned to saccades or fixations, the saccade- and fixation-onset ERPs were plotted as a function of saccade durations (Fig. 2C,D, respectively). When saccade-onset ERPs (aligned to saccade onset) were plotted against changing saccade durations (Fig. 2C), it was evident that the resulting ERPs remained aligned to saccade onset for varying saccade durations (i.e., vertical alignment of the contour plot in Fig. 2C), suggesting that the response was aligned to saccade onset. To confirm this, the fixation-onset ERPs were plotted against preceding saccade durations (i.e., duration of the saccade preceding each fixation) in a plot aligned to fixation onset (Fig. 2D). In this plot, the observed fixation ERPs were still aligned to the saccade onset and not to the fixation onset (i.e., diagonal alignment of the contour plot in Fig. 2D), further suggesting that the observed response was indeed a saccade-aligned response. Since the neural response to eye movements was determined to be aligned to saccade-onset, only the saccade-onset and image-onset ERPs were further analyzed.

Analysis and Removal of the Peri-Saccadic Transient

Saccade-onset ERPs across all analyzed electrodes contained a rapid transient response with a peak just prior to the onset of the saccade response (Fig. 2A; Fig. 3A,B left panel) which is known to arise from extraocular muscle contraction (Yuval-Greenberg et al. 2008; Jerbi et al. 2009; Kovach et al. 2011). This is clearly evident in Figure 2C as the sharp brief voltage transient aligned to onset of saccade. Therefore, it was important to confirm that this transient was a volume-conducted potential that is not part of the MTL response. To determine if this peak arose from volume conduction of muscle activity from the extraocular muscles, the spatial distribution of the peak-to-peak voltage of this transient was plotted across all the intracranial electrodes (see Supplementary Material, Fig. S1 for a representative patient). These spatial distributions revealed that the transient was largest in the electrodes closest to the anterior temporal poles, which are also the ones closest to the orbit, providing strong evidence for this transient reflecting the potential associated with ballistic eye movements (electrooculogram—EOG). Plotting the root-mean-squared (RMS) amplitude of this peri-saccadic transient as a function of distance from the eyes showed that the amplitude of the transient decayed exponentially with increasing distance from the eyes, further suggesting that it is indeed a volume conduction artifact arising from oculomotor activity (see Supplementary Material, Fig. S2 for details). Furthermore, previous work has shown that hippocampal recordings can contain eye movements artifacts, with waveforms and durations

very similar to the transient observed in the current study (Yuval-Greenberg et al. 2008; Kovach et al. 2011). To test the alternate hypothesis that the transient was part of the physiological hippocampal response to eye movements, simulations were performed to determine whether a theta frequency phase-reset mechanism (which has been previously reported as a potential mechanism through which the hippocampus responds to eye movements; Hoffman et al. 2013; Jutras et al. 2013) can generate a high-frequency transient similar to the one that is seen in this study. The simulations demonstrated that a theta frequency reset mechanism can indeed generate a high-frequency transient depending on what phase the oscillators reset to (Fig. 4A). However, the transient generated through this mechanism did not have the biphasic waveform seen in the saccade-related ERPs, arguing that the peri-saccadic transient seen in the current intracranial data is not generated through theta phase resetting. Interestingly, the simulated data showed broadband phase clustering around stimulus onset, despite being generated using a pure theta phase-reset mechanism (Fig. 4B). This was likely due to the high-frequency transient that was present in the simulated signals (Kramer et al. 2008; Bénar et al. 2010). This suggested that the high-frequency transient present in the recorded MTL response to eye movements would also skew the phase clustering metrics used for comparing the saccade-onset and the image-onset responses, further warranting its removal. Therefore, a modified version of the artifact removal algorithm developed by Kovach and colleagues was used to remove the transient from all further analysis (see Methods section for details) (Kovach et al. 2011; Abel et al. 2016). The removal of this transient substantially reduced peri-saccadic power in the 20–200 Hz frequency band (in a 40 ms window centered around saccade onset), which has been previously reported to be the frequency band in which a majority of the power of the intracranial EOG artifact resides (Kovach et al. 2011). The middle panels of Figure 3A,B show representative and grand-average ERPs from hippocampal electrodes after this peri-saccadic transient was removed. Note that for all succeeding analysis of the saccade-onset response, the ICA-filtered data were used. Blink-related ERPs were not contaminated by the same high-frequency transient that contaminated the saccade-related ERPs (Supplementary Material, Fig. S3), providing further evidence that the peri-saccadic transient described above is likely generated by the intraocular muscles involved in eye movements.

Event-Related Potentials

To compare the temporal dynamics of the MTL response to saccade-onset and image-onset, ERPs were generated for both events. For each selected electrode, we calculated the average of the event-aligned response across all the trials and across all experimental blocks. Nonparametric permutation testing was used to test the significance of this response. Figure 3A shows the ERPs for a representative hippocampal electrode for saccade epochs (left), ICA-filtered saccade epochs (middle), and for image-onset epochs (right). Thirteen out of the 15 (86%) analyzed hippocampal electrodes had a statistically significant peak or trough following saccade onset, and all hippocampal electrodes (100%) had a statistically significant peak or trough following image-onset. Similarly, all parahippocampal (PHG) electrodes (100%) had a significant peak or trough following saccade onset and image-onset (Supplementary Material, Fig. S7). The MTL response (hippocampal/PHG) to saccade onset was more rapid compared with the image-onset response, which is evident from Figure 3. It is important to note that the observed ERPs had different amplitudes across subjects which is evident in other work (Paller and McCarthy 2002) but may also have been influenced by the fact that the current analysis included all stimuli, without separating old and new items and hits and misses, all of which have been shown the influence the amplitude of the image-onset response (Fernandez et al. 1999; Paller and McCarthy 2002; Fell et al. 2004, 2008; Mormann et al. 2005; Montefusco-Siegmund et al. 2017). Blink ERPs were analyzed for all subjects. Blink ERPs were characterized by a large trough $\sim$100 ms following blink onset and had a markedly distinct waveform when compared with the saccade- or image-onset ERPs (Supplementary Material, Fig. S3), suggesting that blink ERPs neither contaminate the saccade-onset nor the image-onset ERPs. To further characterize the difference in the image-onset and saccade-onset responses, the phase clustering following stimulus onset was investigated.

Phase Clustering

If, in the presence of an ongoing oscillation, phase clustering occurs following stimulus onset, then phase resetting is considered to be the mechanism giving rise to the ERP. Hence, ITPC was measured for saccade-aligned epochs and for image-onset–aligned epochs. This measure assesses the distribution of the phase at each time point across trials and gives a value between 0 (no phase clustering, uniform phase distribution) and 1 (complete phase clustering). In this case, the ITPC value has been converted to an $ITPC_z$ value to control for the different number of trials for different electrodes/stimuli. The higher the value of the $ITPC_z$, the higher the phase clustering. As evident from Figure 5, there is a stark contrast in the phase clustering following saccade- and image-onset events. Significant hippocampal phase clustering was observed in the delta (1–3 Hz), theta (4–8 Hz), and alpha (9–14 Hz) frequency bands. Significant hippocampal phase clustering was also observed following image-onset; however, it was largest in the delta frequency band, and small, albeit significant, phase clustering was also observed in the theta and alpha frequency bands. The same analysis performed on all the parahippocampal electrodes (see Supplementary Material, Fig. S5) revealed qualitatively similar results. It should be noted that the ITPC analysis reported here was performed on the ICA-filtered saccade-onset–aligned epochs. When a similar analysis was performed on the original saccade-onset–aligned epochs, broadband phase clustering was observed, likely due to the high-frequency peri-saccadic transient that was present in the original data. Although these results suggest significant phase clustering following image-onset and saccade onset in the mesial temporal lobe structures, phase clustering can also be induced by an additive/evoked response that is added to ongoing oscillations at the onset of the stimuli (Lopour et al. 2013). To differentiate between this additive response and a true phase-reset response, the pre- and post-stimulus power was measured for individual trials and for the ERP.

Power Changes

To investigate whether the observed phase clustering following saccade- and image-onset events was due to a phase reset, the pre- versus post-event power was compared in the individual trials and in the ERP. For a pure phase-reset–dependent ERP, there should be no power changes within each trial, but there should be a significant increase in power following the event in the

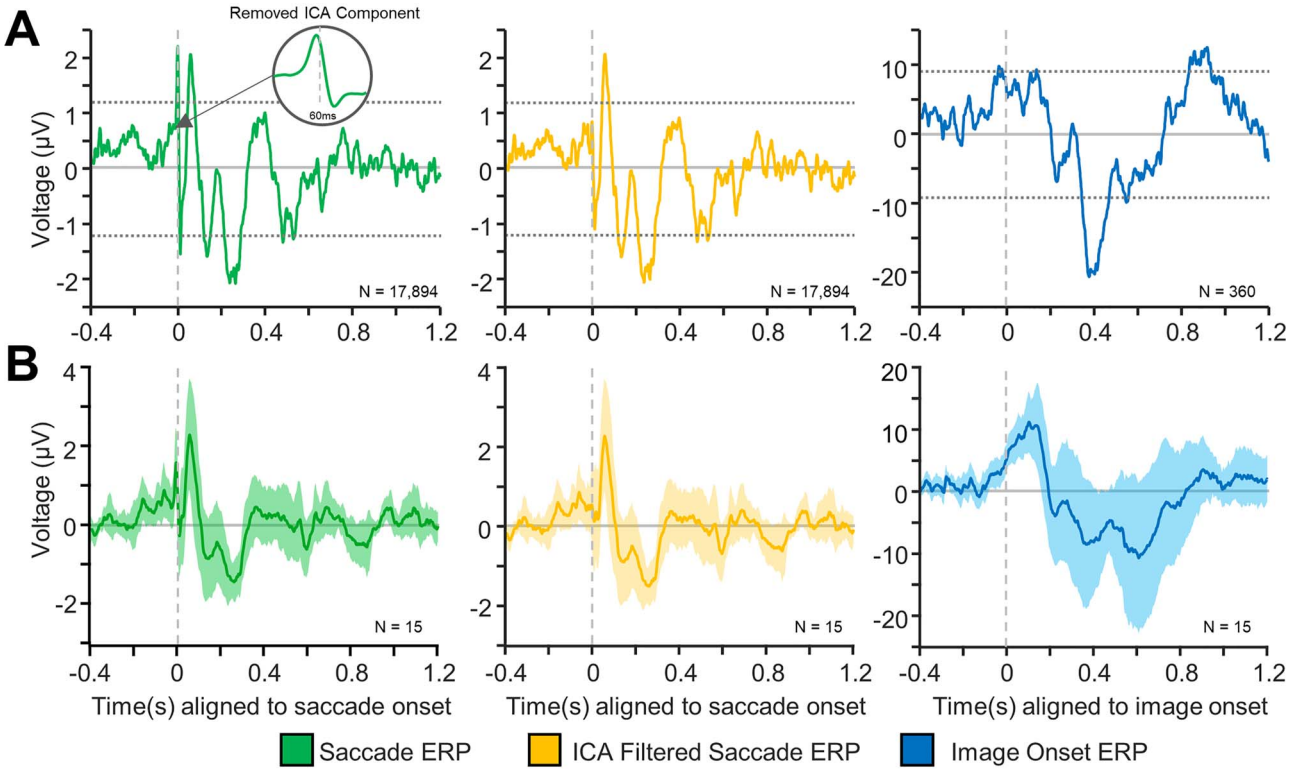

Figure 3. Event-related potentials (ERPs) following saccade- and image-onset. (*A*) Representative ERPs from a hippocampal electrode for saccade-aligned epochs (left), saccade-aligned ICA-filtered epochs (middle), and image-onset–aligned epochs (right) from the same electrode. The dashed horizontal lines mark significance bounds generated using permutation testing (3000 permutations) with randomized polarity inversions (see Methods). The onset in the left-most figure (green) shows the average of the ICA-components (in a 60 ms window surrounding saccade onset) that were removed in order to obtain the ICA-filtered saccade onset ERP. Note that the ICA-filtered ERPs (middle pane) are obtained by removing the peri-saccadic transient from the saccade ERPs (left pane) (see Methods for details). (*B*) Grand-average ERPs for original saccade epochs (left), ICA-filtered saccade epochs (middle), and image-onset (right) epochs. The filled in region indicates 95% confidence intervals for each plot. Note that the ICA filtering successfully removes the transient, peri-saccadic response seen in the saccade-aligned ERPs (middle panel) while maintaining the integrity of the remaining ERP.

ERP. This is precisely what was observed for saccade responses (Fig. 6A). There was no difference in spectral power in the individual trials across any of the frequency bands (Fig. 6Aleft,*C*), but there was a significant broadband increase in power (in the delta, theta, alpha, beta, and low-gamma bands) following saccade onset in the saccade ERP (Fig. 6Aright,*D*). Conversely, all the significant power changes in the image-onset ERP were mirrored by significant power changes in the individual trials (Fig. 6*B*–*D*). This suggests that the image-onset response is not a characteristic phase reset, as there appears to be an addition of power to each individual trial following image-onset, in contrast to the saccade response, which better fits the characteristics of phase resetting across the delta, theta, and alpha frequency bands.

Discussion

In this study, iEEG recorded responses to image presentation, and eye movements were investigated in the human MTL. These responses were characterized by investigating the underlying spectral characteristics of the corresponding ERPs. It was demonstrated that the MTL response following image presentation is a slow, evoked potential with corresponding phase clustering, and power increases primarily in the delta band (Figs 5 and 6). In contrast, the MTL response following eye movements was a faster response with phase clustering but no within-trial power increases. This eye movement response was observed to be aligned to the onset of the saccade and not to the termination of the saccade (fixation) (Fig. 2). These findings suggest that there are distinct mechanisms through which saccade- and image-onset these responses are generated, and the implications of these findings in the context of visual memory are discussed below.

Evoked Image-Onset Response

The image-onset ERP observed in this study was a slower potential than the saccade-related ERP with a first trough occurring at 400–600 ms, similar to the AMTL-N400 response that has been observed in the MTL and the PHG following the presentation of word stimuli (Fernandez et al. 1999; Fell et al. 2004; Mormann et al. 2005, 2007) and had similar temporal characteristics as previously reported MTL response to visual stimuli (Paller and McCarthy 2002) (Fig. 3). Similarly, ERPs associated with probe presentation during a Sternberg task demonstrated a late negative component, similar to this study but without the associated positive p300 component (Kleen et al. 2016).

The image-onset response observed in this study was accompanied by significant phase clustering in the theta and alpha bands. Additionally, the postimage-onset phase clustering was accompanied by an increase in theta and delta power (in

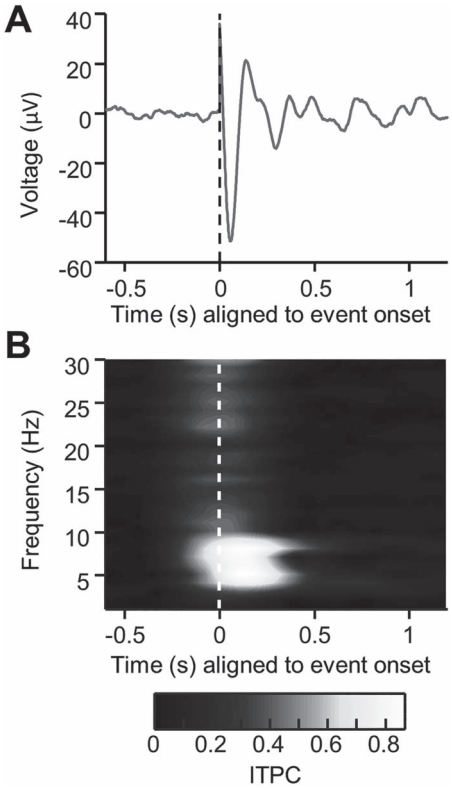

Figure 4. Theta phase-reset simulation. (*A*) An ERP generated by simulating a theta-band phase-reset mechanism (see Methods section). Phase was reset to a preselected phase (in this case, to $^{4}/_{5}\pi$ or 144°). Notice the sharp, high-frequency transient that is present in the ERP at time $t = 0$ despite being generated using a low-frequency phase-reset mechanism. (*B*) The intertrial phase clustering of the same simulated data as in (*A*). Notice that despite the mechanism of the response being a low-frequency reset, broadband phase concentration is seen, suggesting that high-frequency transients in the data can skew intertrial phase clustering metrics to show artificial, high-frequency phase clustering that is not present in the underlying data.

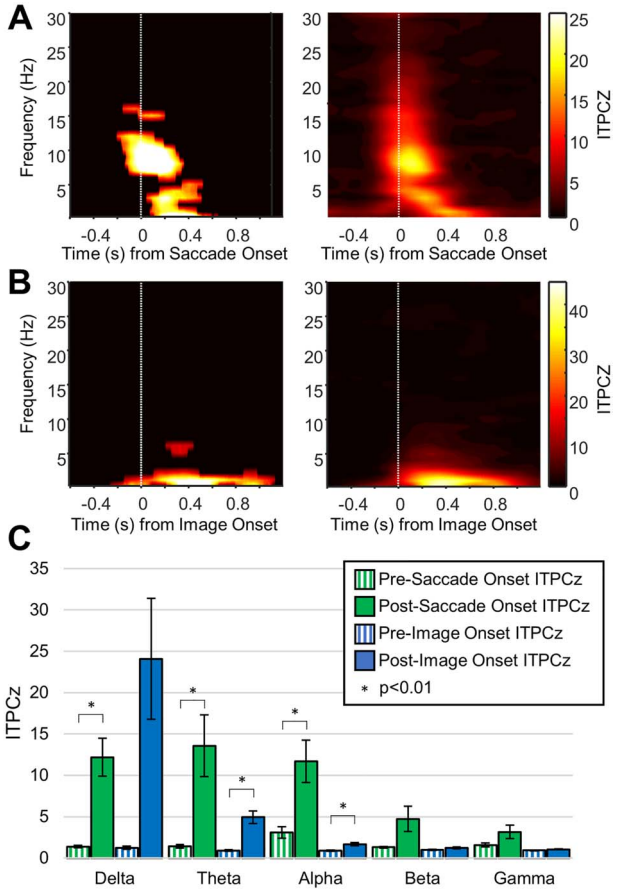

Figure 5. Intertrial phase clustering (ITPC) for hippocampal electrodes. (*A*) Left—Representative $ITPC_z$ for ICA-filtered saccade-aligned epochs. The plot has been masked to indicate significant values (see Methods for details). Right—Grand-average $ITPC_z$ value for ICA-filtered saccade-aligned epochs for all hippocampal electrodes. Note the obvious phase clustering in the delta, theta, and alpha frequency bands. (*B*) Same as A but for image-onset–aligned epochs. Notice that the phase clustering is limited to lower frequency bands and has a longer time course. (*C*) Comparison of $ITPC_z$ values for different time-frequency windows in the pre- and post-event periods (see Table 2). Significant differences are marked with an asterisks.

individual trials and in the ERPs) with a latency of ~250–650 ms. Together these observations suggest that the image-onset response is in large part an evoked response (Fell et al. 2004) and represents recruitment of additional neuronal populations (Mormann et al. 2007). This interpretation is consistent with observations that ERP amplitude, but not phase clustering, is decreased in hippocampal sclerosis (HS) (Mormann et al. 2007). Since the hallmark of HS is CA1 cell loss (Niemeyer 1958), the reduction of the ERP amplitude in HS is likely directly related to the number of CA1 neurons that can be driven to threshold, as well as the number of synaptic contacts that can be made on them. The number of synaptic contacts will directly change the magnitude of the LFP, as it is largely a manifestation of postsynaptic potentials (PSPs), which decrease in HS due to a reduction in the number of available synapses. Furthermore, since phase clustering was not reduced (Mormann et al. 2005, 2007), a decrease in neuronal synchrony is unlikely to explain the decrease in ERP amplitude (Musall et al. 2014) in HS. At the cellular level, it would be expected that an evoked response should be accompanied by an overall increase in cellular firing rates. Indeed studies have shown a marked firing rate increase at image-onset peaking ~ 300 ms after stimulus onset (Andrillon et al. 2015; Mormann et al. 2017), which is consistent with the latency of the image-onset ERP seen here (Fig. 3). Our interpretations regarding the image-onset ERP are consistent with a recent study that demonstrated an image-onset response very similar to the response observed here and characterized it as an additive/evoked response based on the amplitude/power and phase changes discussed earlier (Lopour et al. 2013). In summary, the image-onset response that we observe appears to be a slower potential, with different frequency components than the saccade-related ERP and likely represents an evoked response (Lopour et al. 2013) that involves excitability increases of additional neurons.

Phase Reset Following Saccade Onset

Eye movement-related responses have been previously analyzed following saccade-onset (Jutras et al. 2013; Staudigl et al. 2017) and fixation (Rajkai et al. 2008; Hoffman et al. 2013; Hamamé et al. 2014). Here, we were motivated by the work of Ito and colleagues who have shown that self-initiated saccades during the viewing of natural scenes were associated with phase resetting of the LFP within the beta frequency band or in the

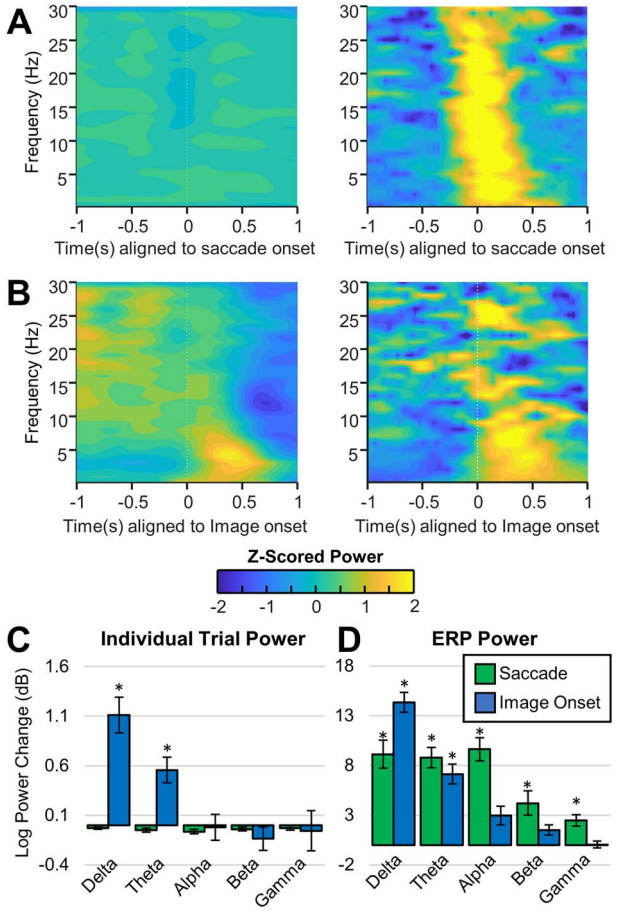

Figure 6. Spectral power for saccade-onset and image-onset epochs for hippocampal electrodes. A and B show power spectrograms in which the power for each frequency has been z-scored to better visualize power changes within each frequency. (A) Left, average power of ICA-filtered individual saccade-aligned epochs across all hippocampal electrodes. Right: Average power of ICA-filtered saccade-aligned ERPs averaged across all hippocampal electrodes. Notice that despite the significant increase in broadband power observed in the saccade ERPs, there is no observable increase in power in the individual trials. (B) Left, average power of individual image-onset–aligned epochs across all hippocampal electrodes. Right: Power of image-onset–aligned ERPs averaged across all hippocampal electrodes. Note that there is an observable increase in delta band and theta band power in the ERP and in the individual trials following image-onset. (C) Average log power change ($10 \log_{10}(\text{post} - \text{event power}/\text{pre} - \text{event power})$) between pre- and post-event time-frequency windows (see Method details for definition of the time-frequency windows). Significant differences are indicated with an asterisks. Notice that there is no significant change in the power following saccade onset, but there is a significant increase in the power of the individual trials in the delta and theta bands following image-onset. (D) Same as C but for the power of the ERP. Note that in the ERPs, there is a significant increase in broadband power following saccade onset and a significant increase in lower frequency power (delta and theta) following image-onset.

theta band with a blank screen in area V1 of the macaque (Ito et al. 2011). Concomitant single-unit recordings disclosed that the resetting was not associated with an increase in spike firing but in fact was explained by a change in spike timing. They concluded that that the early (~75 ms) LFP changes in V1 were likely the manifestation of eye movements associated CDs, whereas single-unit firing rate changes were a manifestation of visual input. Similar findings have been demonstrated in area TE/STS (Purpura et al. 2003; Bartlett et al. 2011) and area V1 (Rajkai et al. 2008) in complete darkness, which suggest that the saccade-related ERP is likely a modulatory input that phase resets ongoing oscillations.

In this context, we have demonstrated that in the human MTL, the saccade-associated ERP represents a phase locking to saccades onset and not its termination (i.e., fixation) (Fig. 2). Like others, we interpret these findings to imply that the postsaccade ERP arises not as a result of visual reafference, but a modulatory input like a CD that is transmitted from gaze control centers to mnemonic structures in addition to a number of other areas of the brain like FEF, TE, V1, and entorhinal cortex (EC) (Sommer and Wurtz 2002, 2008; Purpura et al. 2003; Crapse and Sommer 2008; Ito et al. 2011). Although it may be argued that our LFP analysis is too insensitive to definitively argue the ERP is comprised of a CD, prior work has shown that the saccade-associated LFP is reflective of eye movements, whereas postsaccade firing rate changes reflect visual input (Ito et al. 2011).

Support for the speculation that a CD may be present in mnemonic structures comes from single-unit studies in nonhuman primates (NHP), which have revealed the presence of saccade direction (SD) cells, some of which increase their firing rate as early as 68 ms prior to the saccade (Killian et al. 2015). Previously, the same group reported saccade-related phase resetting of theta oscillations within NHP hippocampus during free viewing, although no LFP data were presented in their more recent paper on SD cells (Killian et al. 2015). It would be interesting to understand if theta phase resetting occurs in the entorhinal cortex of the NHP and the relationship of the SD cells to such ongoing population activity. Nonetheless, their hippocampal phase resetting effect was not associated with increases in spiking rate ((Jutras et al. 2013) Fig. 1*D*), consistent with a modulating effect (as opposed to driving) (Sherman and Guillery 2002) of a CD, as has been previously suggested in area TE of the NHP (Purpura et al. 2003). Such large-scale, crossmodal control via modulating inputs (phase resetting) has been suggested to be mediated through thalamic relay nuclei (Schroeder and Lakatos 2010), which is further supported through anatomical connectivity between the memory and oculomotor networks (Shen et al. 2016). For entorhinal cortex SD cells, such a pathway via LD nucleus of the thalamus has been suggested as the route by which saccade direction information, possibly similar in content to the information transmitted to lateral interparietal sulcus (Duhamel et al. 1992), reaches the entorhinal cortex (Killian et al. 2015). Since the entorhinal cortex represents a major input to the hippocampus (Battaglia et al. 2011), hippocampal phase resetting associated with saccadic eye movements may arise from the transmission of SD cell information to area CA1 of the hippocampus.

That the saccade-related phase resetting starts with the onset of the saccade is a strong evidence that a CD (Purpura et al. 2003; Ito et al. 2011) underlies its generation and argues against visual reafference. Furthermore, our finding that blinks manifest as a starkly different electrophysiological response in the human MTL when compared with the saccade-aligned response (Supplementary Material, Fig. S3) suggests that blink ERPs do not contribute to the saccade-related response in the human MTL. These results further suggesting the saccade-onset ERP is an unadulterated manifestation of a saccade onset related signal, very like a CD. However, additional characteristics of the response would be required to confirm its identity as a CD. Specifically, CDs associated with saccadic eye movements tend to be directional and thus have different waveforms depending on the direction of the saccade (whether it is ipsiversive or contraversive to the recording site). Furthermore, a

saccade-related CD should be present in the dark. Although we have not shown this in our patients since obtaining complete darkness in the clinical setting is problematic, a number of studies have shown that both the LFP (Sobotka and Ringo 1997) and single-unit activity in the NHP hippocampus (Ringo et al. 1994) are modulated by saccades in complete darkness.

Although a number of studies in humans and NHPs have demonstrated both saccade-related ERPs (Hoffman et al. 2013; Jutras et al. 2013), and alterations in single-unit activity with saccadic eye movements (Bartlett et al. 2011), including those recording from the hippocampus, our analyses have allowed us to critically add to this literature by suggesting that the hippocampal ERP is associated with saccade onset, implying that it may arise from a CD (Purpura et al. 2003; Rajkai et al. 2008; Ito et al. 2011). What might be the role of such a CD within the hippocampus? Analogous to the discussion regarding SD cells in the entorhinal cortex (Killian et al. 2015), such saccade direction information may be useful for creating "mnemonic maps" from visual stimuli, a process that requires knowledge of the viewing order, and spatial placement of the visual information. Additionally, CDs in some regions of the brain provide the remapping transformation from the current receptive field (RF) of a neuron to the future field (FF) of the neuron (Duhamel et al. 1992). Envisaging the hippocampus as a comparator (Hasselmo 2005; Vinogradova 2008) of internal representation (via CA3 inputs) to current information (EC → CA1), and in the context of predictive coding (Buckner 2010), the remapping of current RFs to FFs in LIP (Duhamel et al. 1992) may, by analogy, represent the comparison of the future mnemonic representation (prediction) of the visual stimulus to the mnemonic representation of the current visual stimulus within the hippocampus. This remains speculative, and future work will be required to understand the mechanistic role and information provided by such a phase resetting/CD mechanism in the hippocampus beyond the temporal changes in excitability that accompany phase resetting (Hyman et al. 2003; McCartney et al. 2004; Grover et al. 2009; Voloh and Womelsdorf 2016).

Lastly, it is important to note that saccade-related phase resetting was observed in other MTL sites such as the PHG which is known to play a role in visual search behavior (Supplementary Material, Figs S4–S6). For instance, parahippocampal damage has been previously shown to alter visual search behavior, leading to increased number of saccades and visual neglect (Mort et al. 2003; Nemanic et al. 2004). This is consistent with the previously cited literature that suggests anatomically widespread phase resetting associated with saccadic eye movements (Purpura et al. 2003; Ito et al. 2011; Hoffman et al. 2013; Jutras et al. 2013; Staudigl et al. 2017). This is not surprising if such saccade-associated phase resetting is needed for preparing disparate brain regions for processing of new salient visual stimulus for information coding (Canavier 2015), storage (Hyman et al. 2003; McCartney et al. 2004; Grover et al. 2009) and sensory integration (Voloh and Womelsdorf 2016).

Comparison of the Two Responses

The saccade-related ERP stands in stark contrast to the image-onset ERP that we observed, with the image-onset response manifesting as an additive/evoked response, while the saccade response is better described as a phase resetting. At the cellular level, it would be expected that an evoked response should likely demonstrate greater firing rate increases following image-onset, which should occur later in time given its low frequency, whereas the saccade-related ERP would likely not be accompanied by an increase in firing rate, would occur sooner after a saccade than the evoked response, and should show spiking phase locked to the reset oscillation. Although there are limited studies to address this, a human single-unit study by Andrillon et al. (2015) comparing single-unit image-onset responses to saccade-related responses demonstrated a 100% increase in firing rate after image-onset, peaking at 300 ms, while saccade-related responses demonstrated an earlier increase in spiking, and a more modest firing rate increase of 25–30% following a saccade (Andrillon et al. 2015). Additionally, in the NHP hippocampus, an increase in firing rate is seen following image-onset in the same task as the one used here, along with an evoked response and low-frequency phase clustering (Leonard et al. 2015; Montefusco-Siegmund et al. 2017), similar to the response reported in the current study. Although the human single-unit data do suggests a modest increase in firing rate following a saccade, an excess of spike synchrony induced by a modulating input may underlie an increase in apparent firing rate (Ito et al. 2011) following saccades in humans (Andrillon et al. 2015) by biasing spike timing (Cobb et al. 1995; Anastassiou et al. 2011) and not increasing firing rate per se. Lastly and likely most importantly, the LFP is largely a manifestation of postsynaptic potentials, the extent of their synchronization (Buzsáki et al. 2012), and any associated spiking activity (Reimann et al. 2013). Recently, it has been shown that the LFP is an excellent surrogate for predicting the contributions of postsynaptic currents to membrane potential fluctuations (Haider et al. 2016), and specific to our context, Ito and colleagues suggest that the early component of LFP following a saccade is an eye movement-related potential and does not arise from visual reafference. Furthermore, cortical excitation has been observed following a saccadic eye movement in V1 in darkness, which likely arises from a postinhibitory rebound (Ringo et al. 1994; Rajkai et al. 2008). Hence, we suggest that (1) the LFP we observe following a saccadic eye movement has an extrahippocampal origin that modulates the timing of hippocampal spiking but does not directly drive neurons to threshold; (2) it, like the responses in V1, is driven by an initial postsynaptic inhibition followed by rebound excitation (Ringo et al. 1994; Rajkai et al. 2008); (3) the rebound spiking acts nonlocally (i.e., projects to other brain regions) and thus does not contribute to the LFP recorded within the hippocampus, and thus a power increase is not observed early after a saccadic eye movement; and (4) the image-onset response reflects driving inputs from extrahippocampal sites, likely entorhinal cortex, which are known to excite hippocampal neurons through glutamatergic synapses (Amaral and Witter 1989; Yoshida et al. 2008; Battaglia et al. 2011; Suh et al. 2011). Future work will be required to elucidate the validity of these propositions.

Saccade-Related Phase Resetting is not an EOG Artifact

Emerging evidence points to the presence of EOG contamination in iEEG recordings. We have thus endeavored to address this in a number of ways, which led us to conclude that the characteristics of the saccade-related ERPs arise locally within the MTL and are not volume-conducted eye movement artifacts. The various lines of evidence are: (1) The duration of the EOG artifact, which is ~20 ms around saccade onset, cannot contribute to the phase resetting that we observe, since the latencies for the phase resetting are an order of magnitude longer. (2) As evident from a number recent publications (Yuval-Greenberg et al. 2008;

Jerbi et al. 2009; Kovach et al. 2011), EOG artifacts contribute to power increase in the 20–200 Hz frequency band, not within the theta frequency band that we demonstrate our effects in. Since our primary findings are not concerned with these frequency bands, the presence of the artifact is not directly relevant to our findings. (3) We have undertaken a number of additional steps to remove the artifact using the detailed methodology identified by Kovach et al. (2011). The only difference between our artifact removal approach and the one identified by Kovach et al. is that we did not employ bipolar referencing. This decision was not haphazard, since the majority of saccade-related electrophysiology literature employs unipolar referencing and presents our findings consistent with this literature. (4) We demonstrate by analyzing the RMS amplitude of the artifact and that of the resetting response as a function of distance from the eyes (Supplementary Material, Fig. S2); the RMS amplitude of the artifact decays exponentially with distance from the eyes (i.e., proportional to r^{-2}), whereas the RMS amplitude of the response does not. This clear dissociation between the effect we are reporting and the EOG artifact provides unequivocal evidence that the phase resetting response is not artifactual.

Conclusion

In this paper, the field potentials following saccade onset, fixation onset, and image-onset were characterized using the temporal nature of the average MTL response, event-related phase clustering, and spectral power changes. Image-onset responses were shown to have low-frequency phase clustering and within-trial power increases, suggesting an additive/evoked neural response. In contrast, the saccade-related response was aligned to saccade onset, with significant phase clustering across the delta, theta, and alpha bands, and no within-trial power changes consistent with a phase-reset mechanism for the saccadic response. We propose that the saccade-onset response and image-onset response are dichotomous, with the saccade-related response likely representing a CD that modulates hippocampal activity, whereas the image-onset response arises from driving sensory-related signals to the MTL. Future work will require further characterization of saccade-related potentials at behavioral and electrophysiological levels (LFPs and single units), specifically their generation in the dark, their directional dependencies, and the neuronal current sources in these regions. Our work has implications for memory-related testing and neuromodulation, since visual search is likely to engage different hippocampal mechanisms than would visual stimuli presented only during fixation.

Supplementary Material

Supplementary material can be found at *Cerebral Cortex* online.

Author Contributions

Conceptualization, C.K. and T.A.V.; methodology, O.T. and K.H.; software, C.K., O.T., and K.P.; formal analysis, K.P. and C.K.; investigation, O.T., C.K., and K.P.; data curation, O.T., C.K., and K.P.; visualization, K.P.; writing, original draft, C.K. and K.P.; writing, reviewing and editing, C.K., K.P., and T.A.V.; funding acquisition, K.H. and T.A.V.; resources, T.A.V.; supervision, K.H. and T.A.V.

Funding

This work was supported by the National Science and Engineering Research Council (RGPIN-2015-05936 to T.A.V.) and the National Institutes of Health and Brain Canada (grant number 1U01NS103792-01 to T.A.V.). This work was also supported by the Toronto General and Toronto Western Hospital Foundation and the National Science and Engineering Research Council Vanier Canada Graduate Scholarships.

Notes

We would like to acknowledge Victoria Barkley for her help with organizing and assisting with patient data collection. *Conflict of Interest*: Dr. Taufik A. Valiante is an investor in the company Neurescence, that has no involvement in this study. Dr. Taufik A. Valiante provides consulting to the company Panaxium, that has no involvement in this study. David Groppe is now a Clinical Data Scientist at Persyst, which had no involvement in this study

References

Abel TJ, Rhone AE, Nourski KV, Ando TK, Oya H, Kovach CK, Kawasaki H, Howard MA, Tranel D. 2016. Beta modulation reflects name retrieval in the human anterior temporal lobe: an intracranial recording study. *J Neurophysiol*. 115:3052–3061.

Amaral DG, Witter MP. 1989. The three-dimensional organization of the hippocampal formation: a review of anatomical data. *Neuroscience*. 31:571–591.

Anastassiou CA, Perin R, Markram H, Koch C. 2011. Ephaptic coupling of cortical neurons. *Nat Neurosci*. 14:217–224.

Andersson R, Larsson L, Holmqvist K, Stridh M, Nyström M. 2017. One algorithm to rule them all? An evaluation and discussion of ten eye movement event-detection algorithms. *Behav Res Methods*. 49:616–637.

Andrillon T, Nir Y, Cirelli C, Tononi G, Fried I. 2015. Single-neuron activity and eye movements during human REM sleep and awake vision. *Nat Commun*. 6:7884.

Axmacher N, Cohen MX, Fell J, Haupt S, Dümpelmann M, Elger CE, Schlaepfer TE, Lenartz D, Sturm V, Ranganath C *et al*. 2010. Intracranial EEG correlates of expectancy and memory formation in the human hippocampus and nucleus accumbens. *Neuron*. 65:541–549.

Axmacher N, Mormann F, Fernández G, Elger CE, Fell J. 2006. Memory formation by neuronal synchronization. *Brain Res Rev*. 52:170–182.

Bartlett AM, Ovaysikia S, Logothetis NK, Hoffman KL. 2011. Saccades during object viewing modulate oscillatory phase in the superior temporal sulcus. *J Neurosci*. 31:18423–18432.

Battaglia FP, Benchenane K, Sirota A, Pennartz CM, Wiener SI. 2011. The hippocampus: hub of brain network communication for memory. *Trends Cogn Sci*. 15:310–318.

Beauchamp MS, Lee KE, Argall BD, Martin A. 2004. Integration of auditory and visual information about objects in superior temporal sulcus. *Neuron*. 41:809–823.

Bell AJ, Sejnowski TJ. 1995. An information-maximization approach to blind separation and blind deconvolution. *Neural Comput*. 7:1129–1159.

Bénar CG, Chauvière L, Bartolomei F, Wendling F. 2010. Pitfalls of high-pass filtering for detecting epileptic oscillations: a technical note on "false" ripples. *Clin Neurophysiol*. 121:301–310.

Brewer J, Zhao Z, Desmond J, Glover G, Gabrieli JD. 1998. Making memories: brain activity that predicts how well visual experience will be remembered. *Science*. 281:1185–1187.

Buckner RL. 2010. The role of the hippocampus in prediction and imagination. *Annu Rev Psychol*. 61(27–48):C1–C8.

Buzsáki G, Anastassiou C A., Koch C. 2012. The origin of extracellular fields and currents — EEG, ECoG, LFP and spikes. *Nat Rev Neurosci*. 13:407–420.

Canavier CC. 2015. Phase-resetting as a tool of information transmission. *Curr Opin Neurobiol*. 31:206–213.

Chau VL, Murphy EF, Rosenbaum RS, Ryan JD, Hoffman KL. 2011. A flicker change detection task reveals object-in-scene memory across species. *Front Behav Neurosci*. 5:58.

Cobb SR, Buhl EH, Halasy K, Paulsen O, Somogyi P. 1995. Synchronization of neuronal activity in hippocampus by individual GABAergic interneurons. *Nature*. 378:75–78.

Corrigan BW, Gulli RA, Doucet G, Martinez-Trujillo JC. 2017. Characterizing eye movement behaviors and kinematics of non-human primates during virtual navigation tasks. *J Vis*. 17:1–22.

Crapse TB, Sommer MA. 2008. Corollary discharge across the animal kingdom. *Nat Rev Neurosci*. 9:587–600.

Davis P. 1939. Effects of acoustic stimuli on the waking human brain. *J Neurophysiol*. 2:494–499.

Delorme A, Makeig S. 2004. EEGLAB: an open source toolbox for analysis of single-trial EEG dynamics including independent component analysis. *J Neurosci Methods*. 134:9–21.

Duhamel J-RR, Colby CL, Goldberg ME. 1992. The updating of the representation of visual space in parietal cortex by intended eye movements. *Science*. 255:90–92.

Fell J, Dietl T, Grunwald T, Kurthen M, Klaver P, Trautner P, Schaller C, Elger CE, Fernández G. 2004. Neural bases of cognitive ERPs: more than phase reset. *J Cogn Neurosci*. 16:1595–1604.

Fell J, Ludowig E, Rosburg T, Axmacher N, Elger CE. 2008. Phase-locking within human mediotemporal lobe predicts memory formation. *Neuroimage*. 43:410–419.

Fernandez G, Effern A, Grunwald T, Pezer N. 1999. Real-time tracking of memory formation in the human rhinal cortex and hippocampus. *Science*. 285:1582–1585.

Groppe DM, Bickel S, Dykstra AR, Wang X, Mégevand P, Mercier MR, Lado FA, Mehta AD, Honey CJ. 2017. iELVis: an open source MATLAB toolbox for localizing and visualizing human intracranial electrode data. *J Neurosci Methods*. 281:40–48.

Grover LM, Kim E, Cooke JD, Holmes WR. 2009. LTP in hippocampal area CA1 is induced by burst stimulation over a broad frequency range centered around delta. *Learn Mem*. 16:69–81.

Haider B, Schulz DPPA, Häusser M, Carandini M. 2016. Millisecond coupling of local field potentials to synaptic currents in the awake visual cortex. *Neuron*. 90:35–42.

Hamamé CM, Vidal JR, Perrone-Bertolotti M, Ossandón T, Jerbi K, Kahane P, Bertrand O, Lachaux JP, Hamamé CM, Vidal JR *et al*. 2014. Functional selectivity in the human occipitotemporal cortex during natural vision: evidence from combined intracranial EEG and eye-tracking. *Neuroimage*. 95:276–286.

Hanslmayr S, Klimesch W, Sauseng P, Gruber W, Doppelmayr M, Freunberger R, Pecherstorfer T, Birbaumer N. 2007. Alpha phase reset contributes to the generation of ERPs. *Cereb Cortex*. 17:1–8.

Hasselmo ME. 2005. The role of hippocampal regions CA3 and CA1 in matching entorhinal input with retrieval of associations between objects and context: theoretical comment on Lee et al. (2005). *Behav Neurosci*. 119:342–345.

Hoffman KL, Dragan MC, Leonard TK, Micheli C, Montefusco-Siegmund R, Valiante TA. 2013. Saccades during visual exploration align hippocampal 3-8 Hz rhythms in human and non-human primates. *Front Syst Neurosci*. 7:43.

Hyman JM, Wyble BP, Goyal V, Rossi CA, Hasselmo ME. 2003. Stimulation in hippocampal region CA1 in behaving rats yields long-term potentiation when delivered to the peak of theta and long-term depression when delivered to the trough. *J Neurosci*. 23:11725–11731.

Ito J, Maldonado P, Singer W, Grun S, Grün S. 2011. Saccade-related modulations of neuronal excitability support synchrony of visually elicited spikes. *Cereb Cortex*. 21:2482–2497.

Jackson O, Schacter DL. 2004. Encoding activity in anterior medial temporal lobe supports subsequent associative recognition. *Neuroimage*. 21:456–462.

Jerbi K, Freyermuth S, Dalal S, Kahane P, Bertrand O, Berthoz A, Lachaux JP. 2009. Saccade related gamma-band activity in intracerebral EEG: dissociating neural from ocular muscle activity. *Brain Topogr*. 22:18–23.

Johnson EL, Knight RT. 2015. Intracranial recordings and human memory. *Curr Opin Neurobiol*. 31:18–25.

Jutras MJ, Fries P, Buffalo EA. 2013. Oscillatory activity in the monkey hippocampus during visual exploration and memory formation. *Proc Natl Acad Sci U S A*. 110:13144–13149.

Killian NJ, Potter SM, Buffalo EA. 2015. Saccade direction encoding in the primate entorhinal cortex during visual exploration. *Proc Natl Acad Sci U S A*. 112:15743–15748.

Kleen JK, Testorf ME, Roberts DW, Scott RC, Jobst BJ, Holmes GL, Lenck-Santini P-P. 2016. Oscillation phase locking and late ERP components of intracranial hippocampal recordings correlate to patient performance in a working memory task. *Front Hum Neurosci*. 10:1–14.

Klimesch W, Hanslmayr S, Sauseng P, Gruber WR. 2006. Distinguishing the evoked response from phase reset: a comment to Mäkinen et al. *Neuroimage*. 29:808–811.

Kovach CK, Tsuchiya N, Kawasaki H, Oya H, Howard MA, Adolphs R. 2011. Manifestation of ocular-muscle EMG contamination in human intracranial recordings. *Neuroimage*. 54:213–233.

Kramer MA, Tort ABL, Kopell NJ. 2008. Sharp edge artifacts and spurious coupling in EEG frequency comodulation measures. *J Neurosci Methods*. 170:352–357.

Leonard TK, Hoffman KL. 2017. Sharp-wave ripples in primates are enhanced near remembered visual objects. *Curr Biol*. 27:257–262.

Leonard TK, Mikkila JM, Eskandar EN, Gerrard JL, Kaping D, Patel SR, Womelsdorf T, Hoffman KL. 2015. Sharp wave ripples during visual exploration in the primate hippocampus. *J Neurosci*. 35:14771–14782.

Long NM, Burke JF, Kahana MJ. 2014. Subsequent memory effect in intracranial and scalp EEG. *Neuroimage*. 84:488–494.

Lopour BA, Tavassoli A, Fried I, Ringach DL. 2013. Coding of information in the phase of local field potentials within human medial temporal lobe. *Neuron*. 79:594–606.

Makeig S, Westerfield M, Jung T-P, Enghoff S, Townsend J, Courchesne E, Sejnowski TJ. 2002. Dynamic brain sources of visual evoked responses. *Science*. 295:690–694.

McCartney H, Johnson AD, Weil ZM, Givens B. 2004. Theta reset produces optimal conditions for long-term potentiation. *Hippocampus*. 14:684–687.

McCormick C, St-Laurent M, Ty A, Valiante TA, McAndrews MP. 2015. Functional and effective hippocampal-neocortical connectivity during construction and elaboration of autobiographical memory retrieval. *Cereb Cortex*. 25:1297–1305.

Meister MLR, Buffalo EA. 2016. Neurobiology of learning and memory getting directions from the hippocampus: the neural connection between looking and memory. *Neurobiol Learn Mem*. 134:135–144.

Merkow MB, Burke JF, Kahana MJ. 2015. The human hippocampus contributes to both the recollection and familiarity components of recognition memory. *Proc Natl Acad Sci U S A*. 112:14378–14383.

Montefusco-Siegmund R, Leonard TK, Hoffman KL. 2017. Hippocampal gamma-band synchrony and pupillary responses index memory during visual search. *Hippocampus*. 27: 425–434.

Mormann F, Fell J, Axmacher N, Weber B, Lehnertz K, Elger CE, Fernandez G, Fernández G. 2005. Phase/amplitude reset and theta-gamma interaction in the human medial temporal lobe during a continuous word recognition memory task. *Hippocampus*. 15:890–900.

Mormann F, Fernández G, Klaver P, Weber B, Elger CE, Fell J. 2007. Declarative memory formation in hippocampal sclerosis: an intracranial event-related potentials study. *Neuroreport*. 18:317–321.

Mormann F, Kornblith S, Cerf M, Ison MJ, Kraskov A, Tran M, Knieling S, Quian Quiroga R, Koch C, Fried I. 2017. Scene-selective coding by single neurons in the human parahippocampal cortex. *Proc Natl Acad Sci U S A*. 114:1153–1158.

Mort DJ, Malhotra P, Mannan SK, Rorden C, Pambakian A, Kennard C, Husain M. 2003. The anatomy of visual neglect. *Brain*. 126:1986–1997.

Musall S, Von Pfost V, Rauch A, Logothetis NK, Whittingstall K, Von Pföstl V, Rauch A, Logothetis NK, Whittingstall K. 2014. Effects of neural synchrony on surface EEG. *Cereb Cortex*. 24:1045–1053.

Nemanic S, Alvarado MC, Bachevalier J. 2004. The hippocampal/-parahippocampal regions and recognition memory: insights from visual paired comparison versus object-delayed nonmatching in monkeys. *J Neurosci*. 24:2013–2026.

Niemeyer P. 1958. The transventricular amygdalohippocampectomy in temporal lobe epilepsy. In: Baldwin M, Bailey P, editors. *Temporal lobe epilepsy*. Springfield: Charles C. Thomas, pp. 461–482.

Paller KA, McCarthy G. 2002. Field potentials in the human hippocampus during the encoding and recognition of visual stimuli. *Hippocampus*. 12:415–420.

Purpura KP, Kalik SF, Schiff ND. 2003. Analysis of perisaccadic field potentials in the occipitotemporal pathway during active vision. *J Neurophysiol*. 90:3455–3478.

Rajkai C, Lakatos P, Chen CM, Pincze Z, Karmos G, Schroeder CE. 2008. Transient cortical excitation at the onset of visual fixation. *Cereb Cortex*. 18:200–209.

Reimann MW, Anastassiou CA, Perin R, Hill SL, Markram H, Koch C. 2013. A biophysically detailed model of neocortical local field potentials predicts the critical role of active membrane currents. *Neuron*. 79:375–390.

Rey HG, Ison MJ, Pedreira C, Valentin A, Alarcon G, Selway R, Richardson MP, Quian QR. 2015. Single-cell recordings in the human medial temporal lobe. *J Anat*. 227:394–408.

Ringo JL, Sobotka S, Diltz MD, Bunce CM. 1994. Eye movements modulate activity in hippocampal, parahippocampal, and inferotemporal neurons. *J Neurophysiol*. 71:1285–1288.

Salvucci DD, Goldberg JH. 2000. Identifying fixations and saccades in eye-tracking protocols. In: *Proceedings of the symposium on eye tracking research and applications—ETRA '00*. pp. 71–78.

Sauseng P, Klimesch W, Gruber WR, Hanslmayr S, Freunberger R, Doppelmayr M. 2007. Are event-related potential components generated by phase resetting of brain oscillations? A critical discussion. *Neuroscience*. 146:1435–1444.

Schroeder CE, Lakatos P. 2010. Low-frequency neuronal oscillations as instruments of sensory selection. *Trends Neurosci*. 32:9–18.

Sederberg PB, Schulze-Bonhage A, Madsen JR, Bromfield EB, McCarthy DC, Brandt A, Tully MS, Kahana MJ. 2006. Hippocampal and neocortical gamma oscillations predict memory formation in humans. *Cereb Cortex*. 17:1190–1196.

Shah AS, Bressler SL, Knuth KH, Ding M, Mehta AD, Ulbert I, Schroeder CE. 2004. Neural dynamics and the fundamental mechanisms of event-related brain potentials. *Cereb Cortex*. 14:476–483.

Shen K, Bezgin G, Selvam R, McIntosh AR, Ryan JD. 2016. An anatomical interface between memory and oculomotor systems. *J Cogn Neurosci*. 28:1772–1783.

Sherman SM, Guillery RW. 2002. The role of the thalamus in the flow of information to the cortex. *Philos Trans R Soc B Biol Sci*. 357:1695–1708.

Sobotka S, Ringo JL. 1997. Saccadic eye movements, even in darkness, generate event-related potentials recorded in medial sputum and medial temporal cortex. *Brain Res*. 756:168–173.

Sommer MA, Wurtz RH. 2002. A pathway in primate brain for internal monitoring of movements. *Science*. 296:1480–1482.

Sommer MA, Wurtz RH. 2008. Brain circuits for the internal monitoring of movements. *Annu Rev Neurosci*. 31:317–338.

Staudigl T, Hartl E, Noachtar S, Doeller CF, Jensen O. 2017. Saccades phase-locked to alpha oscillations in the occipital and medial temporal lobe enhance memory encoding. *PLoS Biol*. 15:1–15.

Suh J, Rivest AJ, Nakashiba T, Tominaga T, Tonegawa S. 2011. Entorhinal cortex layer III input to the hippocampus is crucial for temporal association memory. *Science*. 334:1415–1420.

Tesche CD, Karhu J. 2000. Theta oscillations index human hippocampal activation during a working memory task. *Proc Natl Acad Sci U S A*. 97:919–924.

Tukey JW. 1977. Exploratory data analysis. Reading (MA): Addison-Wesley.

Vinogradova OS. 2008. Hippocampus as comparator: role of the two input and two output systems of the hippocampus in selection and registration of information. 72:1285–1286.

Voloh B, Womelsdorf T. 2016. A role of phase-resetting in coordinating large scale neural networks during attention and goal-directed behavior. *Front Syst Neurosci*. 10:18.

Womelsdorf T, Valiante TA, Sahin NT, Miller KJ, Tiesinga P. 2014. Dynamic circuit motifs underlying rhythmic gain control, gating and integration. *Nat Neurosci*. 17:1031–1039.

Yoshida M, Fransén E, Hasselmo ME. 2008. mGluR-dependent persistent firing in entorhinal cortex layer III neurons. *Eur J Neurosci*. 28:1116–1126.

Yuval-Greenberg S, Tomer O, Keren AS, Nelken I, Deouell LY. 2008. Transient induced gamma-band response in EEG as a manifestation of miniature saccades. *Neuron*. 58:429–441.